Biomaterials Science

ROYAL SOCIETY OF CHEMISTRY

PAPER

View Article Online
View Journal | View Issue

Cite this: *Biomater. Sci.*, 2021, **9**, 7194

The innate immune response of self-assembling silk fibroin hydrogels

Natalia Gorenkova,[a,b,c] Manfred F. Maitz,[d] Georg Böhme,[b,d] Hani A. Alhadrami,[a,e] Essam H. Jiffri,[a,e] John D. Totten,[a,b] Carsten Werner,[d,f] Hilary V. O. Carswell[b] and F. Philipp Seib *[b,d,g]

Silk has a long track record of use in humans, and recent advances in silk fibroin processing have opened up new material formats. However, these new formats and their applications have subsequently created a need to ascertain their biocompatibility. Therefore, the present aim was to quantify the haemocompatibility and inflammatory response of silk fibroin hydrogels. This work demonstrated that self-assembled silk fibroin hydrogels, as one of the most clinically relevant new formats, induced very low blood coagulation and platelet activation but elevated the inflammatory response of human whole blood *in vitro*. *In vivo* bioluminescence imaging of neutrophils and macrophages showed an acute, but mild, local inflammatory response which was lower than or similar to that induced by polyethylene glycol, a benchmark material. The time-dependent local immune response *in vivo* was corroborated by histology, immunofluorescence and murine whole blood analyses. Overall, this study confirms that silk fibroin hydrogels induce a similar immune response to that of PEG hydrogels, while also demonstrating the power of non-invasive bioluminescence imaging for monitoring tissue responses.

Received 14th June 2021,
Accepted 13th September 2021

DOI: 10.1039/d1bm00936b

rsc.li/biomaterials-science

1. Introduction

Bombyx mori silkworm farming (sericulture) is an established route for the production of the silk fibroin protein and is currently the only source of silk approved for routine medical use in humans.[1,2] The clinical history of the silk protein biopolymer, most notably its use as a suture, spans several millennia. The ability to unwind the silk cocoon to release the silk thread was a critical innovation that supported this use of silk in load-bearing applications (*e.g.* sutures, surgical meshes).[1]

Today, robust protocols exist to generate a liquid silk feedstock[3] that forms the basis for numerous novel silk formats aimed at tackling currently unmet healthcare needs.[1,4] For example, silk fibroin hydrogels are particularly promising because these materials can serve both as an extracellular matrix mimetic[5] or as a release reservoir for therapeutic payloads.[6,7] Proposed applications include, but are not limited to, anticancer drug delivery,[6,8] pancreatic islet transplantation,[9,10] soft[11,12] and hard tissue[13] engineering and tissue fillers (Silk Medical Aesthetics, Inc. Medford, MA, USA; ClinicalTrials.gov Identifier NCT04085822). The Food and Drug Administration (USA) recently approved the first reverse-engineered silk fibroin product (Silk Voice®, Sofregen Inc, Medford, MA, USA) for use in humans in the treatment of vocal fold medialisation and vocal fold insufficiency. Silk Voice® serves as a soft tissue bulking agent and its application protocol is minimally invasive, consisting of injection *via* prefilled silk fibroin syringes coupled to a catheter system.

Silk fibroin can undergo a solution-gel transition following a number of triggers, including a drop in pH, ions, a change in solvation status or an increase in biopolymer kinetics.[14] Increased kinetics can be obtained by vortexing or sonication, which exposes the hydrophobic silk fibroin blocks, thereby promoting hydrogen bond formation and ultimately converting the silk fibroin structure from a random coil to an antiparallel β-sheet with inter-chain physical cross links.[6] Exploiting the ability of silk fibroin to self-assemble utilises Nature's solu-

[a]*King Fahd Medical Research Center, King Abdulaziz University, P.O. BOX 80402, Jeddah 21589, Saudi Arabia*
[b]*Strathclyde Institute of Pharmacy and Biomedical Sciences, University of Strathclyde, 161 Cathedral Street, Glasgow, G4 0RE, UK. E-mail: philipp.seib@strath.ac.uk; Fax: +44 (0) 141 552 2562; Tel: +44 (0)141 548 2510*
[c]*I.M. Sechenov First Moscow State Medical University, 8-2 Trubetskaya street, Moscow, 119991, Russian Federation*
[d]*Leibniz Institute of Polymer Research Dresden, Max Bergmann Center of Biomaterials Dresden, Hohe Straße 6, 01069 Dresden, Germany*
[e]*Department of Medical Laboratory Technology, Faculty of Applied Medical Sciences, King Abdulaziz University, P.O. BOX 80402, Jeddah 21589, Saudi Arabia*
[f]*Technische Universität Dresden, Center for Regenerative Therapies Dresden (CRTD), Fetscherstraße 105, 01307 Dresden, Germany*
[g]*EPSRC Future Manufacturing Research Hub for Continuous Manufacturing and Advanced Crystallisation (CMAC), University of Strathclyde, Technology and Innovation Centre, Glasgow G1 1RD, UK*

tion for robust macromolecular self-assembly and thus eliminates the need for harsh solvents, chemicals or UV-activated cross linkers. Nevertheless, these latter strategies have also been applied to silk fibroin to endow silk hydrogels with novel functions.[15] However, these steps incur biocompatibility risks, as residual solvents or unreacted cross linkers can leach from the silk hydrogel, while UV exposure is incompatible with therapeutic proteins or cells.

The simplicity of physically cross-linked silk fibroin hydrogels is a key asset in translating this technology from the bench to patients, as clinical approval is based on a Substantially Equivalent Device classification. Nonetheless, material biocompatibility is context specific and is influenced by the application route and site, as well as quantity and material format—attributes that need consideration in the context of the ultimate intended use of the material.[1] These additional requirements, in turn, support pioneering work that strengthens the field while, most importantly, ultimately safeguarding patients. For example, we[16,17] and others[18,19] have assessed the performance of self-assembling silk fibroin hydrogels in both healthy and stroked rodent brains with the ultimate goal of exploiting silk fibroin hydrogels as a minimally invasive cell delivery matrix for stroke. Others have explored silk fibroin hydrogel injections as a tool to modulate preterm birth; this included a preliminary four-day biocompatibility study of silk hydrogel.[20] Silk-treated animals showed granulocyte and eosinophil infiltration at the injection site, with a similar moderate inflammatory response to that observed for polyethylene terephthalate sutures (the current clinical standard for treatment of preterm birth).[20]

Other studies have also reported a consistent biocompatibility of subcutaneously implanted silk fibroin hydrogels (*e.g.* ref. 6 and 21). Silk fibroin hydrogels are also used for hard tissue engineering applications (reviewed in ref. 13). For example, silk fibroin hydrogels outperformed polylactide-*co*-glycolide controls in a critical bone defect animal model without inducing an overt tissue response.[22] Overall, these studies have provided histological assessments of the tissue response and now provide a useful performance baseline.

However, quantitative data on physically cross-linked silk fibroin hydrogels and their comparison to hydrogel standards are absent. In addition, studies on additional indicators, such as human haemocompatibility, are currently lacking, even though blood–material interactions and the subsequent inflammatory responses are intimately linked. This link is now emerging as an important indicator of clinical performance.[23,24]

Iatrogenic injury occurring during material placement typically trigger a sequence of events involving haemostasis, acute inflammation, chronic inflammation and the foreign body reaction. Vascular damage and exposure of the implanted material to blood are very early but common triggers of these events.[25] Immediate blood protein adsorption (the Vroman effect)[26] at the implanted material interface forms a provisional signalling matrix, and this material–blood matrix interface initiates a humoural response (*e.g.* the complement system). During the acute inflammatory response, neutrophils are the first responders and are the dominating cell type for the initial 24 to 48 hours. As inflammation continues, macrophages are recruited and their presence can be long lived (*i.e.* months).[25] However, the exact sequence and the extent of these events remain unclear for silk.

Therefore, the aim of the present study was to quantify the haemocompatibility of silk fibroin hydrogels and their capacity for induction of the inflammatory response following subcutaneous administration in immune-competent mice. We included control hydrogels fabricated from synthetic polyethylene glycol (PEG) as a benchmark material. PEG does not actively regulate tissue regeneration and is therefore a useful marker for the baseline tissue response. We used non-invasive bioluminescence imaging, as well as histological assessments, to quantify the acute and chronic inflammatory responses. Non-invasive imaging using luminol (5-amino-2,3-dihydrophthalazine-1,4-dione sodium salt) enabled the detection of acute inflammation because luminol reacts with the superoxide generated within phagosomes of neutrophils *via* a myeloperoxidase-mediated reaction.[27] Lucigenin (bis-*N*-methylacridinium nitrate) also detects superoxide but is activated by phagocyte NADPH oxidase.[27] We also conducted full blood counts, as well as supplementary *in vitro* human blood compatibility studies, to assess the inflammatory and haemostasis responses towards silk fibroin hydrogels, again using PEG hydrogels as a reference material (Fig. 1).

2. Materials and methods

2.1 Silk fibroin hydrogel manufacture

A silk solution from *Bombyx mori* cocoons was prepared as described previously;[28] a visual protocol format showing

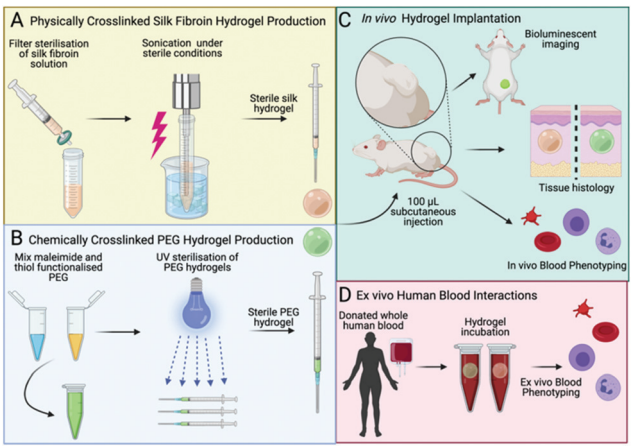

Fig. 1 Schematic of hydrogel fabrication, implantation and *in vivo*/*in vitro* analyses. A. Physically crosslinked silk fibroin hydrogels were manufactured by sonicating a filter sterilised silk fibroin solution. B. Chemically crosslinked PEG hydrogels were manufactured from PEG-thiol and PEG-maleimide. C. Hydrogels were implanted in BALB/c mice using subcutaneous injection (100 µL). A combination of *in vivo* (bioluminescent imaging, blood profiling, immunohistochemical staining). D. *In vitro* analyses with human whole blood were used to assess the performance of silk fibroin hydrogels when compared to PEG hydrogels.

reverse engineering of silk cocoons is available.[29] Briefly, cut cocoons were boiled for 60 min in 20 mM Na_2CO_3 and then rinsed in ddH_2O to remove sericin proteins. The extracted silk fibroin was air dried, dissolved in 9.3 M LiBr at 60 °C and dialyzed (molecular weight cut-off 3500 g mol^{-1}) against ddH_2O to remove the LiBr salt. Next, sufficient 10× phosphate buffered saline (PBS) was added to the silk fibroin solution to obtain physiological osmolarity of the final preparation. The resulting 4% w/v silk fibroin solution was filter sterilised (33 mm Millex-GP syringe filter fitted with a polyether sulfone membrane containing 0.22 μm pores). The solution-gel transition was induced by sonicating the silk fibroin solution with a Branson Digital Sonifier probe sonicator (HD 2070, Bandelin, Berlin, Germany) fitted with a 23 cm long sonication tip (0.3 cm diameter tip and tapered over 8 cm) at 15% amplitude for 15 to 45 seconds. Silk fibroin undergoing the solution-gel transition was aseptically filled into 1 mL syringes, hermetically sealed and stored at 4 °C until *in vivo* use. For *in vitro* human blood studies, 150 μl of silk fibroin (3, 4 and 5% w/v) undergoing the solution-gel transition were transferred to the caps of 2 mL Eppendorf tubes.

2.2. Polyethylene glycol (PEG) hydrogel manufacture

The polymers were purchased from JenKem Technology USA Inc. (Plano, TX, USA). The PEG hydrogel synthesis and characterisation has been reported previously.[30,31] Briefly, four-armed PEG maleimide (10 700 g mol^{-1}, polydispersity 1.03) was added to four-armed methoxy PEG thiol (10 600 g mol^{-1}, polydispersity 1.03) at an equimolecular 1.5 μmol μl^{-1} ratio to PBS pH 5.5. For *in vivo* studies, the polymerising solution was transferred to 1 mL syringes. The PEG hydrogel was buffered to physiological pH by adding an equivalent volume of PBS pH 8.5 to the syringe, followed by UV sterilisation. For *in vitro* human blood studies, 150 μl was transferred to the caps of 2 mL Eppendorf tubes and buffered with PBS.

2.3 Human whole blood analysis

All human studies were approved by the ethics board and complied with institutional and international guidelines (review board of Sächsische Landesärztekammer, ref. EK-BR-24/18-1). All blood donors provided written informed consent. We ensured that donors had not taken any nonsteroidal anti-inflammatory drugs over the past 10 days and were not on any other medications that could interfere with coagulation or inflammatory responses. A non-pathological blood cell count and C reactive protein below 10 μg mL^{-1} (Diagnostik Nord GmbH, Schwerin, Germany) served as further entrance criteria.

Blood was drawn from two AB0-compatible healthy male and female volunteers, immediately anticoagulated with heparin (1.5 IU mL^{-1}) and pooled. Next, 1800 μL of the pooled blood was filled into 2 mL Eppendorf tubes using triplicate sample sets. The tubes were closed with caps containing the respective hydrogel, and the samples were overhead rotated at 12 revolutions per min at 37 °C, 5% CO_2 for 2 h. After incubation, the blood was processed for analysis as described before.[32–34] The study was repeated once, using two different blood donors. For scanning electron microscopy, analysis caps containing hydrogels were dehydrated in increasing ethanol concentrations, critical point dried, gold sputtered and inspected by scanning electron microscopy as detailed before.[34]

2.4 *In vivo* experimental design

All procedures complied with the UK Animals (Scientific Procedures) Act 1986 Amendment Regulations 2012, followed the ARRIVE guidelines and were subjected to review by the Institutional Animal Care and Use Committee at the University of Strathclyde. All *in vivo* studies were approved by the Home Office of the United Kingdom (Project Licence Number PPL 70/8801).

Female nulliparous Balb/c mice, 8 weeks of age, were purchased from Charles River UK Limited. At the time of surgery, the mice were anaesthetised using isoflurane and randomly assigned to receive either a PEG hydrogel or a self-assembling silk fibroin hydrogel or neither. The injection site at the centre of the lower dorsum was shaved and cleaned, and a single 100 μl subcutaneous hydrogel injection was administered (Fig. 1C). The experimenter was blinded to the experimental groups. At 3 h post injection, the first non-invasive bioluminescence imaging was performed. Either luminol (100 mg kg^{-1}; Sigma-Aldrich Company Ltd, Gillingham, UK) or 10-methyl-9-(10-methylacridin-10-ium-9-yl)acridin-10-ium dinitrate (lucigenin [25 mg kg^{-1}]; Abcam, Cambridge, UK) were injected intraperitonially to monitor the acute and delayed inflammatory response, respectively.[27] Luminol and lucigenin substrate stock solutions were prepared in normal saline, filter-sterilised and stored at −20 °C.

Mice were imaged at the maximum signal intensity (at the 15 min post-injection time point, *F*/stop = 1 and binning = 16) using a Xenogen IVIS 200 imaging system controlled by Living Image Software 4.3.1 (Caliper Life Sciences). The IVIS Imaging Systems software package version 4.2 (Caliper Life Sciences, Xenogen Corp. 2007) was used to calculate the peak total bioluminescent signal by applying standardised regions of interest. Data were presented as total flux in photons per second per region of interest. Macroscopic images were captured with a Samsung Galaxy Neo camera, CMOS 16.0 MP resolution, with f/1.9 aperture.

2.5 Mouse whole blood analysis

Animals were randomly selected at the indicated time points (post-implantation days 2 and 35) from the silk fibroin hydrogel group, the PEG hydrogel group, and the untreated control group. All animals were dosed with sodium pentobarbital (60 mg kg^{-1} i.p.) and maintained under isoflurane for arterial blood sampling *via* cardiac puncture. Whole blood (approx. 400 μL per animal) was collected with a 22-gauge needle, drawn into a 1 mL heparinised syringe and then transferred into EDTA collection tubes (Kabe Labortechnik GmbH Nümbrecht, Germany). Blood samples were subjected to full blood counts on the day of collection at the Veterinary

Diagnostic Services, University of Glasgow. Samples were analysed using a Siemens Advia 120 automated haematology analyser (Erlangen, Germany). For each sample, a blood smear was also examined after staining with Romanowsky and May-Grünwald Giemsa stains, and a manual white blood cell differential count was conducted based on 200 leukocytes.

2.6 Mouse histology and immunofluorescence

At the indicated time points, the animals were euthanised by cervical dislocation and samples were collected and fixed in 4% w/v paraformaldehyde for 24 h. The samples were then immersed in cryoprotective solution (30% w/v sucrose in PBS with 0.05% w/v sodium azide) for 72 h, followed by rapid freezing on dry ice. Coronal cryostat sections were cut (20 μm thickness) throughout the implant territory. The tissue samples were stained with haematoxylin and eosin (H&E), and collagen deposition was visualised by trichrome staining.

For immunohistochemistry, sections were incubated in 10% (v/v) blocking serum in PBS containing 0.3% v/v Triton X-100 for 40 min prior to overnight incubation with the primary CD11b antibody (1 : 200, ab1211, Abcam, Cambridge, UK) at 4 °C to detect macrophages. After incubation with the primary antibody, the sections were washed three times for 5 min in PBS and then incubated for 2 h with an Alexa-488 secondary antibody (1 : 500 dilution, Invitrogen, ThermoFisher Scientific, Waltham, MA, USA). The sections were rinsed three times for 5 min in PBS before application of Vectashield antifade mounting medium with DAPI (Vector Laboratories Ltd, Peterborough, UK). Images were captured and analysed using WinFluor V3.9.1 (Nikon Eclipse E600).

2.7 Statistical analyses and data files

Data were plotted and analysed as detailed previously.[35] Briefly, sample pairs were analysed using Welch's independent *t*-test while multiple groups were analysed by one-way ANOVA with a Bonferroni *post-hoc* test (Prism 9.2.0; GraphPad Software Inc., San Diego, CA, USA). Asterisks were used to denote statistical significance as follows: $*P < 0.05$, $**P < 0.01$, $***P < 0.001$. All data were presented as mean values ± standard deviation (SD). The number of independent experiments (n) is noted in each figure legend. All data created during this research are openly available from the University of Strathclyde Pure, at https://dx.doi.org/10.15129/09ab2ef9-03e0-470e-a7aa-496cab1a8f60.

3. Results

The performance of the silk fibroin hydrogel was assessed *in vivo* in mice and *in vitro* using human whole blood (Fig. 2). The *in vitro* human whole blood analysis showed no signs of haemolysis in any of the samples. The prothrombin F1 + 2 fragment served as a biomarker for coagulation activation, and its levels were low across all samples and similar to the blank control. The control and 5% w/v hydrogel treatments levels were similar, and PEG and 3 & 4% w/v silk hydrogels showed slightly higher activation states (Fig. 2A). An increasing solid content of the silk fibroin hydrogels (*i.e.* from 3 to 5% w/v) further decreased coagulation activation (Fig. 2). Platelet activation was monitored by quantifying platelet decay and leukocyte–platelet conjugate formation; both these markers were low for all hydrogel samples and for the control group (Fig. 2B and C).

The inflammatory response was monitored using C5a as a complement activation marker. The complement fragment C5a concentration was always higher for silk fibroin hydrogels than for the PEG hydrogel; however, both hydrogel types induced higher C5a levels than were seen for the blank reference control (Fig. 2D). The C5a pattern was similar to the CD11b expression pattern (*i.e.* a marker for granulocyte and monocyte activation) (Fig. 2E). Both hydrogel types induced a similar extent of granulocyte decay (approximately 30%) and leukocyte activation (approximately 60%) (Fig. 2E and F). Though the scanning electron microscopy assessment was challenging because the hydrogel thickness compromised image quality, we were able to observe that all silk fibroin hydrogels were densely covered with granulocytes, whereas the PEG hydrogel showed mainly dehydration and crystallisation artefacts (Fig. 2G).

The PEG and silk fibroin hydrogels injected subcutaneously into mice were both readily visible by visual inspection (data not shown). The PEG hydrogels retained their shape over the course of the study, while the silk fibroin hydrogels showed progressive shape loss from day 7 onwards. The systemic biocompatibility of self-assembling silk fibroin hydrogels was assessed by determining full blood counts (Fig. 3). For both hydrogels, the performance across all 17 measured parameters showed very similar trends, with no statistically significant differences between them. Comparison of these blood values with the untreated control animals showed a similar trend across these parameters (Fig. 3). However, platelets were significantly raised at day 2 for PEG hydrogels and at day 35 for both silk fibroin and PEG when compared to untreated control mice.

The inflammatory response of hydrogels was monitored longitudinally in the mice. We used non-invasive bioluminescence imaging to assess both acute and chronic inflammation using the luminol and lucigenin substrates, respectively.[27] The acute inflammatory signal for the silk fibroin group was low and remained low throughout the study (Fig. 4A). By contrast, the PEG hydrogel group showed a significantly higher inflammatory response, especially at 3 hours. However, over the first two days of the study, this acute inflammatory response subsided and reached the low levels observed for the silk group.

The chronic inflammatory response for both hydrogel types was similar, although this varied among the hydrogel samples (Fig. 4B). For example, silk hydrogels showed a significantly higher signal at days 2, 7 and 14 than the PEG hydrogel. At day 36 the chronic inflammatory signal for both hydrogel types showed no statistically significant differences. Overall, the

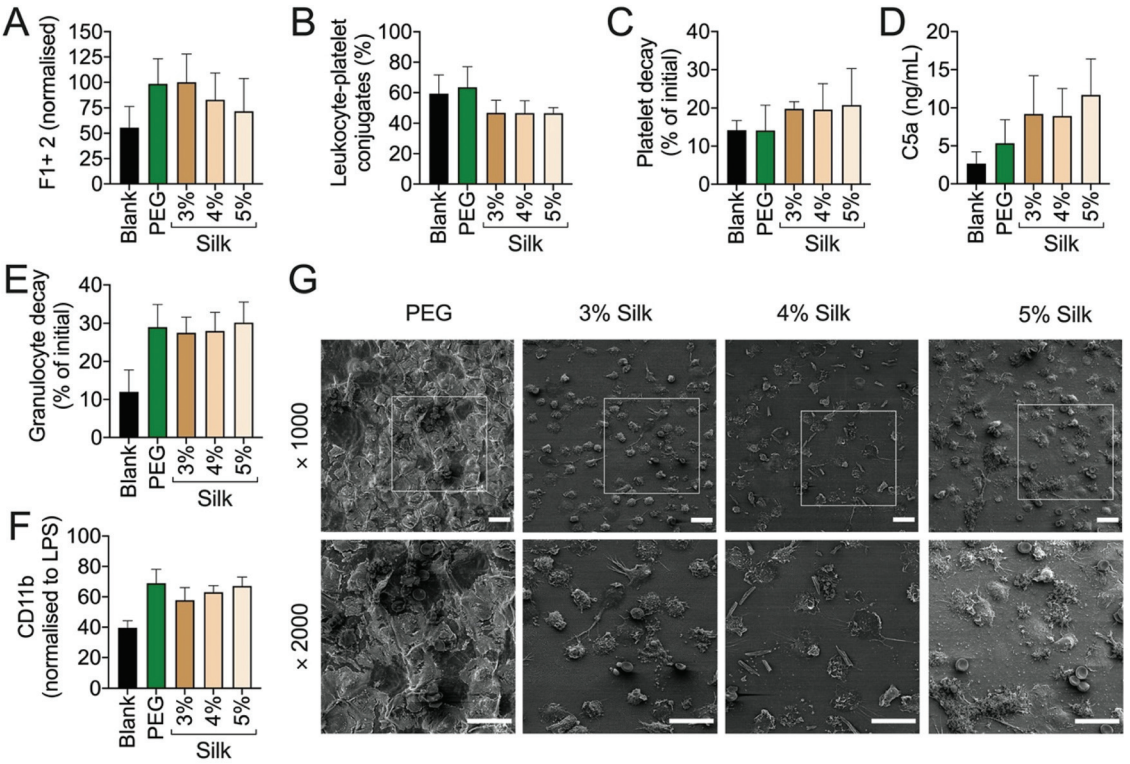

Fig. 2 *In vitro* whole human blood interactions with silk and PEG hydrogels. PEG or 3–5% silk fibroin hydrogels were incubated for 2 h at 37 °C with whole human blood and subsequently analysed for markers of haemostasis (A–C) or inflammation (D–F). G. Representative scanning electron microscopy images of PEG or 3–5% silk fibroin hydrogels following blood incubation. Scale bars: 20 μm. Triplicate measurements were averaged from two independent blood donors.

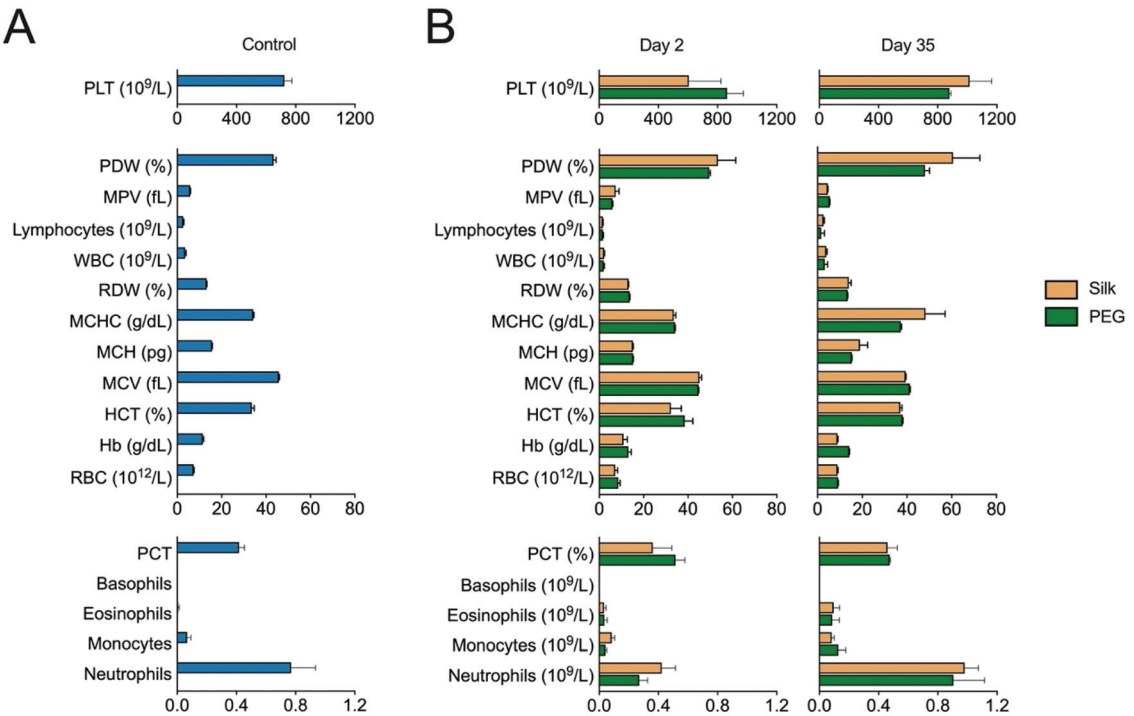

Fig. 3 *In vivo* whole blood analysis following hydrogel implantation. Blood counts conducted on samples drawn from BALB/c (A) control mice and (B) mice 2 days and 35 days post implantation of silk or PEG hydrogels ($n \geq 3$ per hydrogel group except PEG day 35 $n = 2$). Platelets (PLT); platelet distribution width (PDW); mean platelet volume (MPV); white blood cell (WBC), red cell distribution width (RDW); mean corpuscular hemoglobin concentration (MCHC); mean corpuscular hemoglobin (MCH); mean corpuscular volume (MCV); hematocrit (HCT); haemoglobin (Hb); red blood cell (RBC), procalcitonin (PCT).

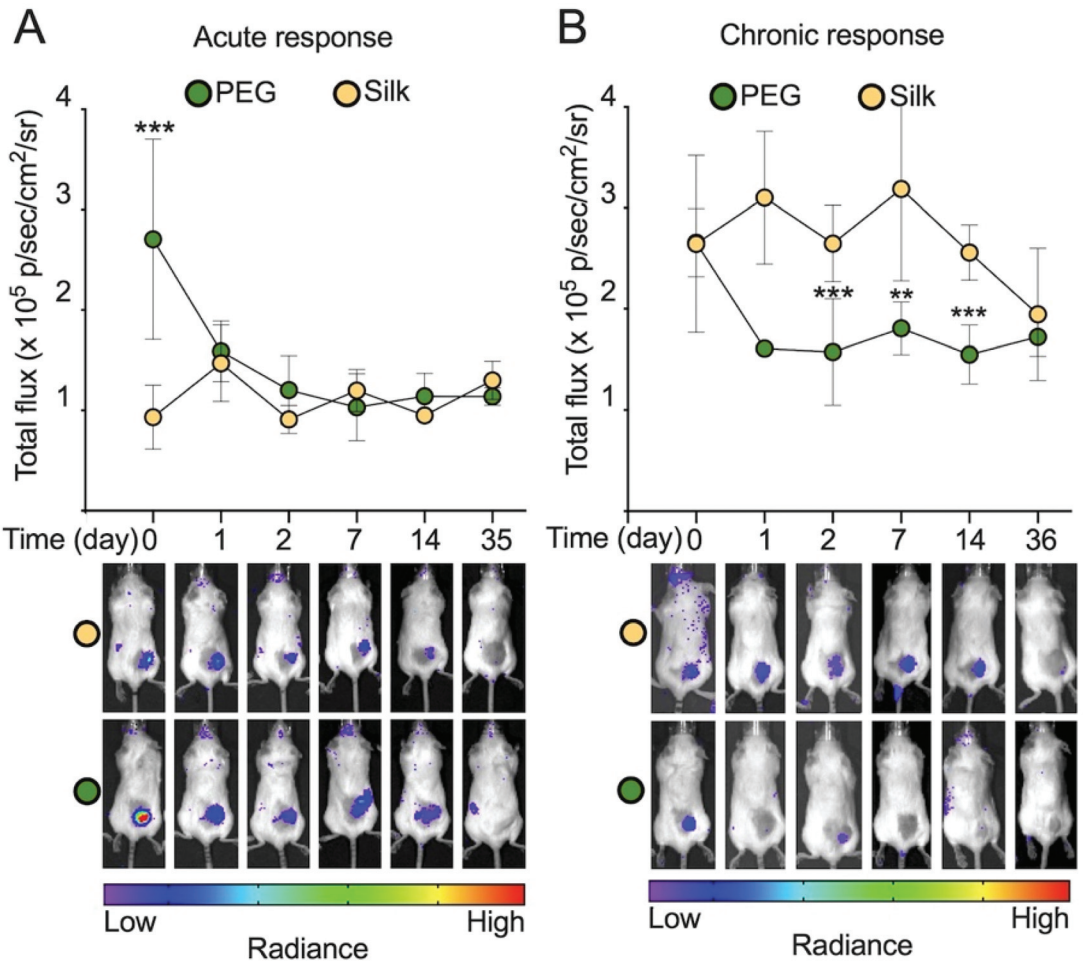

Fig. 4 Non-invasive imaging of the acute and chronic inflammatory response towards implanted silk fibroin and PEG hydrogels. A. Acute response (*i.e.* luminol bioluminescence) in BALB/c mice measured at three hours (day 0) and later time points. Silk: day 0 (n = 8), 1 (n = 10), 2 (n = 10), 7 (n = 5), 14 (n = 5), 35 (n = 5). PEG: day 0 (n = 5), 1 (n = 5), 2 (n = 5), 7 (n = 5), 14 (n = 5), 35 (n = 5). B. Chronic response (*i.e.* lucigenin bioluminescence) in BALB/c mice measured at three hours (day 0) and later time points. Silk: day 0 (n = 10), 1 (n = 10), 2 (n = 10), 7 (n = 9), 14 (n = 5), 36 (n = 5). PEG: day 0 (n = 5), 1 (n = 5), 2 (n = 5), 8 (n = 5), 15 (n = 5), 36 (n = 5). Error bars are hidden in the plot symbol when not visible.

chronic inflammatory signal for both samples was low over the study course.

We included histological assessment to corroborate the bioluminescence data sets. At day 2, both hydrogels were intact (Fig. 5A) and were in close proximity to the adjacent tissues. At these contact sites, intermittent but substantial cell infiltration was evident, with little difference between the hydrogel types (Fig. 5A). Most of the infiltrating cells advanced up to 200 μm into the hydrogel, although some were present in the core of the hydrogel. At day 35, cells were found throughout the hydrogel, with no apparent differences between silk fibroin and PEG. Both hydrogels showed a uniform cell infiltration, coupled with a close association between the surrounding tissues and the hydrogel (Fig. 5B). However, less cells at the tissue–hydrogel interface appeared lower at day 35 than at day 2. Collagen staining was included to assess the contribution of the hydrogel to extracellular matrix remodelling (Fig. 6). For the silk fibroin hydrogels, some collagen staining was present at both 2 and 35 days (Fig. 6A2 and B1). Active collagen deposition was clearly evident at the tissue–PEG hydrogel interface already on day 2 and individual collagen fibres could be seen (Fig. 6A3). At day 35, PEG hydrogels showed collagen deposition.

The involvement of macrophages, as part of the acute and delayed tissue response, was also assessed by CD11b immunofluorescent staining (Fig. 7). At day 2, numerous macrophages were present at the tissue–hydrogel interface for both hydrogels (Fig. 7A). At day 35, the PEG hydrogels continued to harbour macrophages in the material core while some were also visible within the silk fibroin hydrogel (Fig. 7B). For silk fibroin, macrophages were still present at the tissue–hydrogel interface, albeit in substantially less than day 2. Overall, for both materials, reduced numbers of macrophages were observed at the tissue–hydrogel interface and within the hydrogel after chronic exposure (*i.e.* day 35).

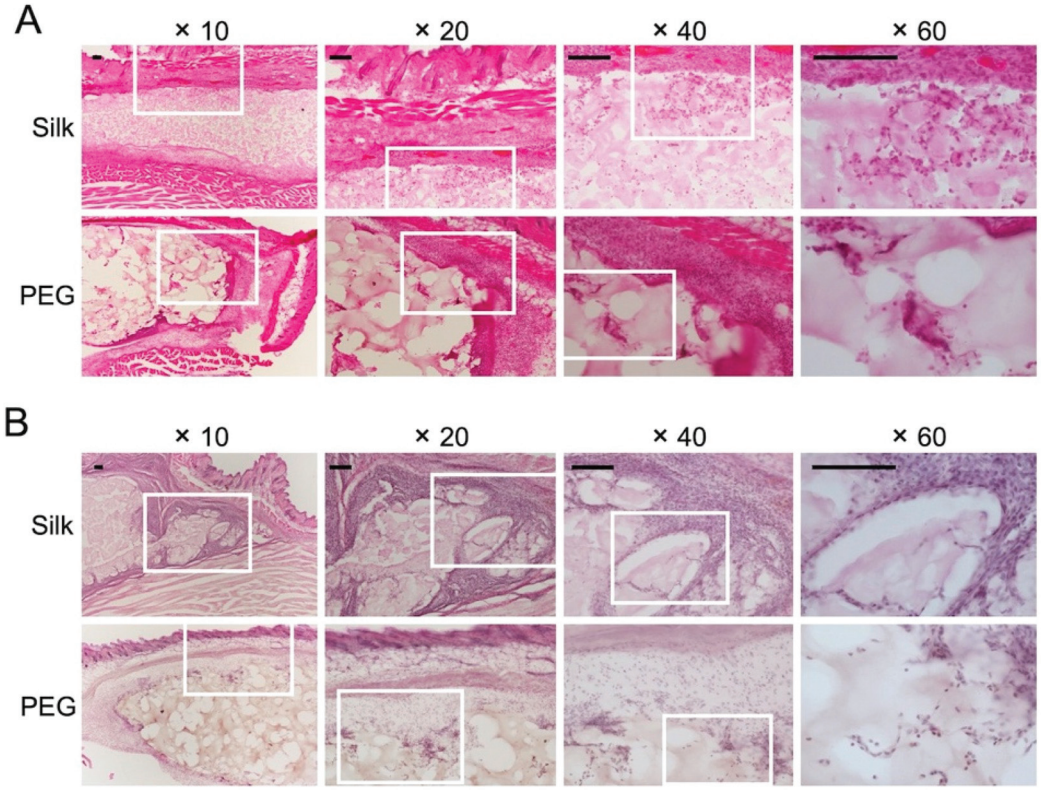

Fig. 5 Histological analyses of hydrogel implants and surrounding tissue. Representative haematoxylin and eosin-stained sections of silk fibroin and PEG hydrogel implants with surrounding tissue at A, day 2 and B, day 35 post implantation. Images taken with ×10, ×20, ×40 and ×60 objective lenses and white boxes are the zoomed areas. Scale bars: 100 μm.

4. Discussion

In a medical context, polymeric hydrogels are often used as bulking agents for aesthetics, tissue engineering applications or carriers for drugs and cells. In addition to synthetic polymers (*e.g.* polyethylene glycol), biopolymers (*e.g.* alginate, collagen and hyaluronic acid) are widely exploited, and many are approved for human use. Our ability to reverse engineer silk into its aqueous format has sparked a renewed interest in this ancient material, including its use in hydrogels.[3] Silk fibroin hydrogels are able to overcome several limitations currently associated with many other biopolymers, including shrinkage, weak mechanics and rapid degradation (or little control over the degradation rate), as well as difficulties in sourcing clinical grade material.[6]

We used Na_2CO_3-mediated degumming to remove sericin because residual sericin is thought to induce an adverse immune response.[1] This degumming strategy is also used to create medical silks.[1] Different processing strategies exist to generate self-assembling silk hydrogels though a common feature is the disruption of the hydrating water shell surrounding crystallisable silk sequences. This disruption ultimately leads to physical crosslinking *via* entanglement and beta sheet formation. In the present study we assessed self-assembling silk hydrogels because they are widely studied and are entering clinical trials. Nonetheless, data sets within the public domain are incomplete. For example, data are lacking regarding silk hydrogel blood compatibility, as well as regarding their systemic and local inflammatory responses. To date quantitative data on physically cross-linked silk fibroin hydrogels and their comparison to hydrogel standards are absent too. We therefore included PEG as a reference material. Iatrogenic injury occurring during material placement typically trigger a sequence of events including haemostasis. Vascular damage and exposure of the implanted material to blood are very early but common triggers of the tissue response.[25] However, reports detailing human haemocompatibility studies are absent, even though blood–material interactions and the subsequent inflammatory responses are intimately linked. In the present study, we conducted two main biocompatibility assessments: *in vitro* human whole blood experiments and *in vivo* experiments on the systemic and local inflammatory responses towards silk hydrogels in mice.

The use of human whole blood is the best *in vitro* setup available to date to evaluate overall blood compatibility, because studies focusing only on either platelet activation, coagulation cascade or inflammatory responses neglect the activating cross-talk between these pathways.[32,36–38] For the purpose of this study, a number of blood compatibility parameters were measured that can be broadly classified as (1) hae-

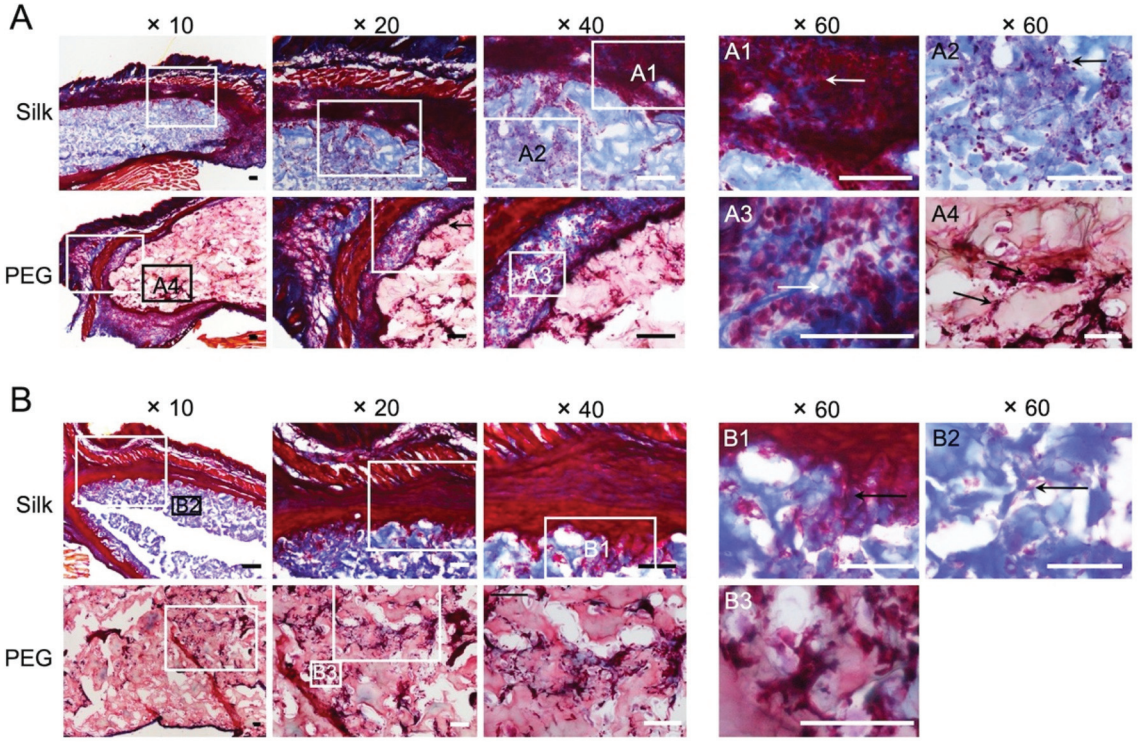

Fig. 6 Histology of hydrogel implants with surrounding tissue remodelling. Representative trichrome stained sections of silk fibroin and PEG hydrogel implants with surrounding tissue at A, day 2 and B, day 35 post implantation. Images taken with ×10, ×20, ×40 and ×60 objective lenses and boxes are the zoomed areas. Scale bars: 100 μm.

mostasis parameters (*e.g.* platelet decay, prothrombin F1 + 2 fragment, leukocyte–platelet conjugates) and (2) inflammatory parameters (*e.g.* C5a, CD11b, granulocyte decay). We included PEG hydrogels as a direct hydrogel reference material. Like PEG, silk fibroin hydrogels also showed a very low haemostasis response, with very low coagulation activation (*i.e.* F1 + 2 fragments) irrespective of the amount of silk present (Fig. 2A).

The very low haemostasis response observed here with silk fibroin hydrogels is in line with earlier *in vitro* human blood compatibilities studies using silk fibroin films and nanoparticles.[32–34] Seminal studies by Motta and co-workers showed that silk processing influenced platelet activation and the macrophage response, as well as plasma protein adsorption. This work has shown lower protein adsorption by silk fibroin films with higher crystallinity and hydrophobicity, especially for factors C3a, C5a and C3b (ref. 39). We previously showed that multiple silk processing factors influenced the biological responses. For example, samples that were water annealed at 25 °C for 6 h showed best blood compatibility, based on haemostasis and inflammatory markers, that was similar to clinically used blood contacting materials (*e.g.* polytetrafluoroethylene).[34] Nonetheless, single parameters, such as β-sheet content, isoelectric point or contact angle, were poor predictors for blood compatibility of silk.[34] Simply extrapolating previous observations from silk films to our hydrogel system is difficult. For example, for this study, silk fibroin hydrogels had a high crystallinity, were fully hydrated and had a low silk content at the blood material interface. The findings presented here therefore help to close a critical gap in the literature.

Silk does not accumulate in the body (or environment), and it degrades into benign products. However, the exact timescale during which silk persists in the body depends on multiple factors, including, but not limited to, the implantation site, the material format, the surface topography, the silk secondary structure and the amount of silk implanted (or the addition of other materials).[1,40] For example, silk fibroin films with a low beta sheet content showed a very rapid onset of film dissolution in less than one hour after implantation. This dissolution process was triggered by tissue moisture rather than proteolytic degradation.[41] By contrast, films with a high beta sheet content were stable for more than 4 weeks *in vivo* and required a cell-mediated degradation mechanism.[41] A ubiquitous tissue response to any implanted material, including silk, arises due to iatrogenic injury occurring during material placement[25] and to the acute inflammatory response mediated by the Vroman effect,[26] where blood serum proteins adsorb to the material surface and become 'contact activated'. The Vroman effect triggers the innate immune response.

This innate immune response is a first-line defence, and tissue-infiltrating neutrophils are the first responders, triggering an inflammatory cascade. The resulting acute inflam-

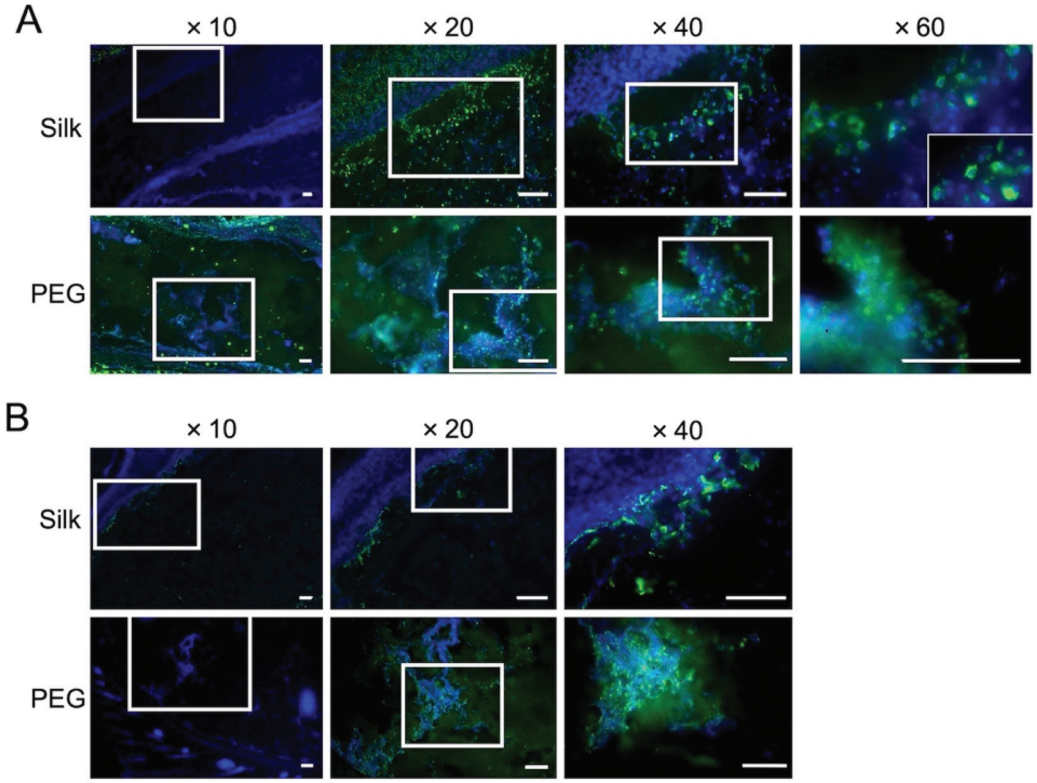

Fig. 7 Macrophage infiltration and retention within silk fibroin and PEG hydrogel implants. Representative CD11b stained sections of silk and PEG hydrogel implants with surrounding tissue at A, day 2 and B, day 35 post implantation. Images taken with ×10, ×20, ×40 and ×60 objective lenses and white boxes are the zoomed areas. Scale bars: 100 μm.

mation is a physiological response mechanism necessary for tissue regeneration and healing. The field of biomaterials typically strives to eliminate complement activation because this activation is an indicator of inflammation. However, a shift has occurred in this paradigm, as recent studies now highlight the importance of complement activation for wound healing and tissue regeneration[23] (reviewed in ref. 24). The innate tissue response can also contribute to material degradation and is believed to make a substantial contribution to the degradation of solution-stable silk formats *in vivo*. For example, in humans, silk surgical meshes typically induce a mild inflammatory response. These meshes degrade over time and are replaced with viable tissue.[42] Nonetheless, systematic *in vivo* studies are needed to provide a comprehensive public record.[43]

Histology is the current standard in the field, although a few studies have also included ultrasound imaging for longitudinal monitoring of material fates.[44,45] We believe that this study is the first to use non-invasive imaging to quantitatively monitor the immune and tissue response. We used neutrophil- and macrophage-specific substrates[27] to monitor their longitudinal responses towards silk fibroin hydrogel over time. The acute neutrophil response to silk fibroin hydrogels was comparable to the response seen with PEG hydrogels, except at 3 hours post administration, when the neutrophil response was significantly lower for silk fibroin hydrogels than for PEG hydrogels (Fig. 3A). Over the remaining 5 weeks of the study, both silk fibroin and PEG hydrogels showed a low neutrophil response, which was corroborated by gross histological examination.

The chronic macrophage response was also monitored over 5 weeks (Fig. 3B). Both silk fibroin and PEG hydrogels showed a consistently low chronic inflammatory response albeit a higher signal for silk at days 1 to 14. No substantial changes were noted in total blood counts.

The favourable tissue response towards silk observed here is also corroborated by the wider scientific literature. For example, comparison of silk fibroin films to the synthetic polystyrene and poly(2-hydroxyethyl)methacrylate polymers showed that silk fibroin adsorbed comparable amounts of human plasma complement fragment C3 and IgG, but lower amounts of fibrinogen.[46] Mononuclear cell activation was significantly lower for silk, as was macrophage adhesion, suggesting a superior biocompatibility of silk over the synthetic polymers.[46] *In vivo* studies also demonstrated a greater inflammatory response to collagen and polylactic acid films than for silk fibroin,[47] although the results were based exclusively on histology and on the use of substrates seeded with mesenchymal stem cells prior to implantation. Mesenchymal stem cells are known to modulate the immune system[48] and could complicate the interpretation of these data.

Others have implanted silk fibroin hydrogels subcutaneously in immune compromised athymic mice (*i.e.* Swiss nude mice). Subsequent histological assessment showed transient eosinophil, neutrophil and macrophage recruitment, resulting in inflammation at 7 and 14 days post implantation. The inflammation subsided by 4 weeks and cleared within 3 months.[21] However, the use of athymic mice complicates the interpretation of the immune response towards silk.

Physically cross-linked silk hydrogels rich in beta sheets persist for several weeks *in vivo*, though the exact timescales are context specific.[6] The importance of silk fibroin hydrogel remodelling, cell infiltration[49] and silk hydrogel degradation[50] are key attributes that impart therapeutic value to silk hydrogels. For example, the use of silk fibroin injections as a treatment for cervical insufficiency in pregnant rabbits augmented the cervix and initiated only a low inflammatory response that was comparable to cerclage treatment. Histology showed a loss of 70% of the silk hydrogel volume over 6 weeks, accompanied by a mild tissue response by macrophages and a small number of neutrophils and eosinophils at days 28 and 42.[51]

Non-invasive imaging has emerged as a complementary tool to histology for monitoring hydrogel degradation.[44,45] However, differentiating material shrinkage from immune cell-mediated degradation is difficult. We therefore believe that the use of neutrophil-specific and macrophage-specific non-invasive bioluminescence imaging is a useful tool for monitoring the *in vivo* responses towards silk. Here, we provide a first example using silk fibroin hydrogels.

One challenge that arises when comparing our work to prior studies is created by the differences in material formats, amounts of implanted silk fibroin and silk processing (*e.g.* degumming time, dissolution medium *etc*.). Emerging evidence suggests that the material format, and not just its composition, impacts the innate immune response.[52] For example, primary human monocytes released more IL-1β and IL-6 in response to three-dimensional silk scaffolds than to two-dimensional silk films when the surface areas were maintained constant. However, no adaptive immune response was observed in peripheral blood T cells from healthy donors.[52]

5. Conclusions

This work demonstrated that silk fibroin hydrogels induced only slight blood coagulation and platelet activation but clearly elevated the inflammatory response of human whole blood. However, this blood response did not reflect a systemic inflammatory response. *In vivo* bioluminescence imaging of neutrophils and macrophages showed an acute, but mild, local inflammatory response. The macrophage response towards silk fibroin hydrogels was mild, peaked at days 1 to 7 and then declined to levels equivalent to those of PEG hydrogels at day 36. This time-dependent immune response was corroborated by histology and immunofluorescence evaluations. We speculate that this tissue response not only contributes to silk hydrogel degradation but also stimulates new tissue formation. Overall, this study confirms that silk fibroin hydrogels elicit similar immune responses to those seen with PEG hydrogels. The findings also demonstrate the power of non-invasive bioluminescence imaging for monitoring tissue immune responses.

Author contributions

N. G. performed all *in vivo* experiments, analysed and interpreted the data. G. B. synthesised PEG hydrogels. M. F. M. performed human blood studies with technical support from Stefanie Hänsel, analysed and interpreted the data. J. D. T. analysed data, discussed the results and generated figures. All authors discussed the results and edited the manuscript. F. P. S. conceived the research study, supervised the work and wrote the manuscript.

Conflicts of interest

There are no conflicts to declare.

Acknowledgements

The authors extend their appreciation to the Deputyship for Research & Innovation, Ministry of Education in Saudi Arabia for funding this research work through the project number (862). The authors would like to thank Anne Goudie for technical assistance.

References

1 C. Holland, K. Numata, J. Rnjak-Kovacina and F. P. Seib, *Adv. Healthcare Mater.*, 2019, **8**, e1800465.
2 G. Janani, M. Kumar, D. Chouhan, J. C. Moses, A. Gangrade, S. Bhattacharjee and B. B. Mandal, *ACS Appl. Bio Mater.*, 2019, **2**, 5460–5491.
3 D. N. Rockwood, R. C. Preda, T. Yucel, X. Wang, M. L. Lovett and D. L. Kaplan, *Nat. Protoc.*, 2011, **6**, 1612–1631.
4 F. P. Seib, *Materials*, 2021, **14**, 1160.
5 S. Phuagkhaopong, L. Mendes, K. Muller, M. Wobus, M. Bornhauser, H. V. O. Carswell, I. F. Duarte and F. P. Seib, *ACS Appl. Mater. Interfaces*, 2021, **13**, 30420–30433.
6 F. P. Seib, *Ther. Delivery*, 2018, **9**, 469–487.
7 S. H. Tran, C. G. Wilson and F. P. Seib, *Pharm. Res.*, 2018, **35**, 248.
8 F. P. Seib, E. M. Pritchard and D. L. Kaplan, *Adv. Funct. Mater.*, 2013, **23**, 58–65.
9 N. Ashari, H. W. Pang, T. Simon, Y. Xiong, J. M. Coburn, J. S. Bromberg, D. L. Kaplan, J. McLenithan and M. J. Fontaine, *Cell. Immunol.*, 2018, **329**, 10–16.

10 N. E. Davis, L. N. Beenken-Rothkopf, A. Mirsoian, N. Kojic, D. L. Kaplan, A. E. Barron and M. J. Fontaine, *Biomaterials*, 2012, **33**, 6691–6697.
11 E. Bellas, B. J. Panilaitis, D. L. Glettig, C. A. Kirker-Head, J. J. Yoo, K. G. Marra, J. P. Rubin and D. L. Kaplan, *Biomaterials*, 2013, **34**, 2960–2968.
12 C. S. Murphy, L. Liaw and M. R. Reagan, *BMC Biomed. Eng.*, 2019, **1**, 27.
13 V. J. Neubauer, A. Döbl and T. Scheibel, *Materials*, 2021, **14**, 674.
14 A. Matsumoto, J. Chen, A. L. Collette, U. J. Kim, G. H. Altman, P. Cebe and D. L. Kaplan, *J. Phys. Chem. B*, 2006, **110**, 21630–21638.
15 X. Mu, V. Fitzpatrick and D. L. Kaplan, *Adv. Healthcare Mater.*, 2020, **9**, e1901552.
16 N. Gorenkova, I. Osama, F. P. Seib and H. V. O. Carswell, *ACS Biomater. Sci. Eng.*, 2019, **5**, 859–869.
17 I. Osama, N. Gorenkova, C. M. McKittrick, T. Wongpinyochit, A. Goudie, F. P. Seib and H. V. O. Carswell, *Sci. Rep.*, 2018, **8**, 13655.
18 L. Fernandez-Garcia, N. Mari-Buye, J. A. Barios, R. Madurga, M. Elices, J. Perez-Rigueiro, M. Ramos, G. V. Guinea and D. Gonzalez-Nieto, *Acta Biomater.*, 2016, **45**, 262–275.
19 L. Fernandez-Garcia, J. Perez-Rigueiro, R. Martinez-Murillo, F. Panetsos, M. Ramos, G. V. Guinea and D. Gonzalez-Nieto, *Front. Cell. Neurosci.*, 2018, **12**, 296.
20 A. S. Critchfield, R. McCabe, N. Klebanov, L. Richey, S. Socrate, E. R. Norwitz, D. L. Kaplan and M. House, *Reprod. Sci.*, 2014, **21**, 1266–1273.
21 O. Etienne, A. Schneider, J. A. Kluge, C. Bellemin-Laponnaz, C. Polidori, G. G. Leisk, D. L. Kaplan, J. A. Garlick and C. Egles, *J. Periodontol.*, 2009, **80**, 1852–1858.
22 M. Fini, A. Motta, P. Torricelli, G. Giavaresi, N. Nicoli Aldini, M. Tschon, R. Giardino and C. Migliaresi, *Biomaterials*, 2005, **26**, 3527–3536.
23 M. Bergmann, C. Jeanneau, T. Giraud, G. Richard and I. About, *Clin. Oral Investig.*, 2020, **24**, 4185–4196.
24 Y. Mödinger, G. Q. Teixeira, C. Neidlinger-Wilke and A. Ignatius, *Int. J. Mol. Sci.*, 2018, **19**, 3367.
25 B. Corradetti, *The immune response to implanted materials and devices*, Springer, 2017.
26 L. Vroman, A. L. Adams, G. C. Fischer and P. C. Munoz, *Blood*, 1980, **55**, 156–159.
27 J. C. Tseng and A. L. Kung, *Chem. Biol.*, 2012, **19**, 1199–1209.
28 S. A. L. Matthew, J. D. Totten, S. Phuagkhaopong, G. Egan, K. Witte, Y. Perrie and F. P. Seib, *ACS Biomater. Sci. Eng.*, 2020, **6**, 6748–6759.
29 T. Wongpinyochit, B. F. Johnston and F. P. Seib, *J. Visualized Exp.*, 2016, **116**, 54669.
30 Y. D. P. Limasale, P. Atallah, C. Werner, U. Freudenberg and R. Zimmermann, *Adv. Funct. Mater.*, 2020, **30**, 2000068.
31 P. Atallah, Y. D. P. Limasale, U. Freudenberg and C. Werner, *Faraday Discuss.*, 2019, **219**, 224–251.
32 M. F. Maitz, C. Sperling, T. Wongpinyochit, M. Herklotz, C. Werner and F. P. Seib, *Nanomedicine*, 2017, **13**, 2633–2642.
33 F. P. Seib, M. Herklotz, K. A. Burke, M. F. Maitz, C. Werner and D. L. Kaplan, *Biomaterials*, 2014, **35**, 83–91.
34 F. P. Seib, M. F. Maitz, X. Hu, C. Werner and D. L. Kaplan, *Biomaterials*, 2012, **33**, 1017–1023.
35 J. D. Totten, T. Wongpinyochit and F. P. Seib, *J. Drug Targeting*, 2017, **25**, 865–872.
36 M. Gorbet, C. Sperling, M. F. Maitz, C. A. Siedlecki, C. Werner and M. V. Sefton, *Acta Biomater.*, 2019, **94**, 25–32.
37 C. Sperling, M. Fischer, M. F. Maitz and C. Werner, *Biomaterials*, 2009, **30**, 4447–4456.
38 M. Weber, H. Steinle, S. Golombek, L. Hann, C. Schlensak, H. P. Wendel and M. Avci-Adali, *Front. Bioeng. Biotechnol.*, 2018, **6**, 99.
39 A. Motta, D. Maniglio, C. Migliaresi, H. J. Kim, X. Wan, X. Hu and D. L. Kaplan, *J. Biomater. Sci., Polym. Ed.*, 2009, **20**, 1875–1897.
40 A. E. Thurber, F. G. Omenetto and D. L. Kaplan, *Biomaterials*, 2015, **71**, 145–157.
41 F. P. Seib and D. L. Kaplan, *Biomaterials*, 2012, **33**, 8442–8450.
42 N. A. Fine, M. Lehfeldt, J. E. Gross, S. Downey, G. M. Kind, G. Duda, D. Kulber, R. Horan, J. Ippolito and M. Jewell, *Plast. Reconstr. Surg.*, 2015, **135**, 339–351.
43 C. Guo, C. Li and D. L. Kaplan, *Biomacromolecules*, 2020, **21**, 1678–1686.
44 X. Leng, B. Liu, B. Su, M. Liang, L. Shi, S. Li, S. Qu, X. Fu, Y. Liu, M. Yao, D. L. Kaplan, Y. Wang and X. Wang, *J. Tissue Eng. Regener. Med.*, 2017, **11**, 822–830.
45 S. Li, D. Yu, H. Ji, B. Zhao, L. Ji and X. Leng, *Biomed. Eng. Online*, 2018, **17**, 87.
46 M. Santin, A. Motta, G. Freddi and M. Cannas, *J. Biomed. Mater. Res.*, 1999, **46**, 382–389.
47 L. Meinel, S. Hofmann, V. Karageorgiou, C. Kirker-Head, J. McCool, G. Gronowicz, L. Zichner, R. Langer, G. Vunjak-Novakovic and D. L. Kaplan, *Biomaterials*, 2005, **26**, 147–155.
48 A. R. R. Weiss and M. H. Dahlke, *Front. Immunol.*, 2019, **10**, 1191.
49 Y. Kambe, A. Murakoshi, H. Urakawa, Y. Kimura and T. Yamaoka, *J. Mater. Chem. B*, 2017, **5**, 7557–7571.
50 Y. Kambe and T. Yamaoka, *Biomater. Sci.*, 2019, **7**, 4153–4165.
51 Y. Zhang, N. Raia, A. Peterson, D. L. Kaplan and M. House, *Tissue Eng., Part A*, 2020, **26**, 379–386.
52 M. Bhattacharjee, E. Schultz-Thater, E. Trella, S. Miot, S. Das, M. Loparic, A. R. Ray, I. Martin, G. C. Spagnoli and S. Ghosh, *Biomaterials*, 2013, **34**, 8161–8171.